NASA Technical Memorandum 86877

Structural and Aeroelastic Analysis of the SR-7L Propfan

Murray Hirschbein, Robert Kielb, Robert Aiello,
Marsha Nall, and Charles Lawrence
Lewis Research Center
Cleveland, Ohio

March 1985

NASA

STRUCTURAL AND AEROELASTIC ANALYSIS OF THE SR-7L PROPFAN

Murray Hirschbein, Robert Kielb, Robert Aiello,
Marsha Nall, and Charles Lawrence
National Aeronautics and Space Administration
Lewis Research Center
Cleveland, Ohio 44135

SUMMARY

This paper presents a structural and aeroelastic analysis of a large scale advanced turboprop rotor blade. This 8-blade rotor is designed to operate at Mach 0.8 at an altitude of 35 000 ft. The blades are highly swept and twisted and of spar/shell construction. Due to the complexity of the blade geometry and its high performance, it is subjected to much higher loads and tends to be much less stable than conventional blades. Four specific analyses were conducted: (1) steady deflection; (2) natural frequencies and mode shapes; (3) steady stresses; and (4) aeroelastic stability. State-of-the-art methods were used to analyze the blades including a large deflection, finite element structural analysis and an aeroelastic analysis including interblade aerodynamic coupling (cascade effects). The study found the blade to be structurally sound and aeroelastically stable. However, it clearly indicated that advanced turboprop blades are much less robust than conventional blades and must be analyzed and fabricated much more carefully in order to assure that they are structurally sound and aeroelastically stable.

INTRODUCTION

When propellers were replaced in commercial aircraft by turbojets, the overall propulsive efficiency was reduced, but the aircraft cruising speed was increased. Since fuel was a small part of the overall operating cost, the increased total passenger or cargo miles that could be provided by a given aircraft with the higher speeds more than made up for the increased fuel consumption. Ever since the drastic rise in fuel costs during the 1970's, a major thrust within the aeronautics community has been to reduce aircraft fuel consumption. The development of low bypass ratio turbofan engines returned some of the lost efficiency without loss of performance and also resulted in more powerful engines. The subsequent development of high-bypass-ratio engines resulted in even further improvements. As part of the overall effort to increase propulsive efficiency even more, the NASA advanced turboprop program has brought the development of commercial aircraft propulsion full circle. The goal of this program is to develop turboprops which can replace turbofans without any appreciable loss in aircraft performance, but with a significant gain in fuel economy. Analytical and experimental studies have shown that fuel savings of 15 to 30 percent are possible compared to today's turbofan engines (ref. 1). These turboprops have 8 to 10 low-aspect-ratio highly-swept blades which are twisted along the span and curved back about the axis of rotation. The forward speed of the aircraft is about Mach 0.8 and the blade tip speed approaches 800 ft/sec. These turboprop blades will operate in a very complicated and severe aeromechanical environment.

Designs such as these have been known for some time, but the means to analyze them and to build them did not exist. Today, with the development of high speed computers and sophisticated engineering software, advanced turboprops can be analytically studied more thoroughly and more accurately. Also, with the development of advanced materials such as fiber reinforced composites, these advanced designs which meet structural and aerodynamic performance requirements are feasible and can be built.

This paper presents a structural and aeroelastic analysis of a prototype, large-scale, advanced turboprop blade which was designed by Hamilton Standard Division of United Technologies Corporation under contract to NASA. The blade (designated SR-7L and shown in fig. 1) is part of a complete 8-blade 9-ft diameter rotor system scheduled to be built, tested and ultimately flown on a test bed aircraft. The results presented in this paper are from independent analyses of SR-7L conducted at the NASA Lewis Research Center.

Blade Description

The SR-7L large scale advanced turboprop blade analyzed in this paper is 47 in long from the bottom of the shank to the tip. The airfoil section is 41 in long. The blade is designed for a cruise Mach number of 0.8 at 35 000 ft altitude with a rotational blade tip speed of 800 ft/sec. The power loading under these conditions is 32.0 shp/ft^2. The blade is of spar/shell construction. The spar is solid aluminum and blends into an integral aluminum shank. The spar is 3.1 in thick at the base of the airfoil section and tapers to a thickness of less than 0.05 in near the blade tip. The shell is of variable thickness and is made from plies of woven fiberglass cloth. Each ply is 0.007 in thick. The blade twist and offset (relative to a radial line) also vary along the span and are shown in figure 2.

An additional construction feature is the nickel sheath along the leading edge of the blade. The purpose of the sheath is to protect the blade against foreign object damage from small hard objects such as stones or hail. The thickness of the sheath varies from a maximum of 0.012 in near the blade leading edge, to 0.006 in where it blends in with the shell. The overall complexity of the blade geometry and construction, along with the high power loading, tip speed and cruise Mach number, make the structural and aeroelastic analyses much more difficult than for a conventional propeller blade.

Analytical Procedure

The objective of this study was to ascertain the structural stability and integrity of the SR-7L blade design by analyzing four key areas of blade response:

(1) Steady state displacements
(2) Natural frequencies and mode shapes
(3) Steady state stresses
(4) Classical flutter

In order to conduct these analyses, a variety of in-house and commercial computer codes were utilized. A brief description of the most significant codes follows:

(1) COBSTRAN - an in-house, special purpose composite mechanics program designed to produce composite-equivalent input data sets for COSMIC NASTRAN and MSC/NASTRAN and to calculate individual ply stresses from NASTRAN output datasets. The composite mechanics in COBSTRAN is fully generalized and contains general failure criteria. However, the code contains streamlined geometric and finite element model algorithms designed specifically for blade-like structures (ref. 2).

(2) COSMIC NASTRAN - a large, general purpose finite element analysis computer program developed for NASA.

(3) MSC/NASTRAN - a commercial version of NASTRAN with enhanced capabilities.

(4) ASTROMIC - an in-house, fast-running classical flutter code designed for preliminary analysis and parametric studies of rotating blade-like structures. The code uses subsonic and supersonic two-dimensional, cascade unsteady aerodynamics and models the structure as a straight, swept (or unswept) beam (ref. 3).

(5) ACA/NASTRAN - a modification of the classical flutter analysis in COSMIC NASTRAN. This enhancement incorporates the effects of cascade unsteady aerodynamics and blade sweep effects into COSMIC NASTRAN which then uses a modal analysis to calculate aeroelastic stability (ref. 4).

(6) EZPLOT - an in-house graphics code streamlined for use with NASTRAN input and output datasets.

In addition to these codes, several special purpose pre- and post-processors were written to provide the proper interfacing between the codes. Furthermore, several modifications had to be made to these major codes or to their solution procedures in order to fully accommodate the very complex geometry and structural behavior of SR-7L.

The overall structural and aeroelastic analyses followed the procedure shown in the flowchart in figure 3. Both analyses started with a geometric/design database for SR-7L. A special preprocessor was used to extract detailed geometric data for the spar and shell in order to build a detailed composite-equivalent finite element model. While this model was being built, distributed beam properties derived from the database were used to build an ASTROMIC model in order to conduct preliminary aeroelastic analyses. These analyses were used to estimate the aeroelastic stability of SR-7L and guide the more refined aeroelastic analyses conducted with ACA/NASTRAN.

The structural and aeroelastic analyses of SR-7L proceeded along essentially, independent paths. The fundamental bridge between the two analyses was the detailed finite element model of the blade.

The approach was to model the spar/shell construction by an equivalent laminated plate model. The shell, adhesive, spar, and shell filler material were taken to be separate layers and were combined to produce equivalent plate properties using the composite mechanics in COBSTRAN. This process, as it applies to SR-7L, will be described in greater detail in the next section. Other approaches, such as merging a separate three-dimensional spar model with

a hollow shell model or generating a combined three-dimensional spar/two-dimensional shell model were considered. However, these two approaches greatly complicated the modeling process and would have necessitated major changes to the finite element modeling algorithms in COBSTRAN. Also, the approach adopted has proven very successful in modeling turbine engine fan blades including superhybrid composite blades and blades with hollow cavities and composite inlays (ref. 5).

Once a COBSTRAN model was built, two NASTRAN input datasets were generated: one for MSC/NASTRAN, and one for COSMIC NASTRAN. Both versions of NASTRAN had to be utilized to analyze the blade structurally and aeroelastically due to the geometrically large deflections that can occur in thin, swept blades such as SR-7L. This has been observed experimentally (ref. 6) and predicted analytically for smaller aerodynamic models (ref. 7). While COSMIC NASTRAN cannot accurately account for this possibility, a modified application of the nonlinear displacement solution capability in MSC/NASTRAN (solution sequence No. 64) was used for detailed analysis of deflections, stresses and natural modes.

On the other hand, a COSMIC NASTRAN input dataset for the COBSTRAN model was needed for use in ACA/NASTRAN. Prior to conducting a detailed aeroelastic analysis with this modified version of COSMIC NASTRAN, blade modal characteristics must be generated elsewhere in the code and supplied to the aeroelastic analysis. COSMIC NASTRAN does not have the capability to rigorously account for large deflections. However, the code can iterate to accurately determine the differential stiffness due to the softening or stiffening effects of non-follower type applied forces acting on the deflected blade. This approach is not as accurate as the fully nonlinear analysis incorporated in MSC/NASTRAN but can be acceptable for calculating reliable stability boundaries provided the discrepancies between the rigorous and approximate analyses are small. For all cases analyzed in this study, the agreement between the approximate and rigorous nonlinear analysis was sufficient to assure that good aeroelastic analyses could be conducted using ACA/NASTRAN. This judgment was based on comparisons of the blade deflections and natural frequencies.

Once the COBSTRAN model of SR-7L was built and the COSMIC NASTRAN structural response was verified against the MSC/NASTRAN response, detailed structural and aeroelastic analyses proceeded independently.

STRUCTURAL ANALYSIS

Finite Element Modeling

The finite element mesh for SR-7L was developed from coordinate descriptions defining the blade spar and shell cross-sectional geometries at 27 stations along the blade span. The midchord line of each cross section was determined from the aerodynamic profile data over a radial span of 10.0 to 54.0 in (as shown in fig. 4). Each midchord line was then represented by 26 grid points defining coordinate values and thicknesses.

COBSTRAN is designed to accept 14 grid point definitions at each radial section along the blade span. Selection of grid points was made to establish a finer mesh along the leading and trailing edges of the spar (as shown in fig. 5).

This was done to minimize the effect of the elements representing a transition of properties between the all-shell nodes and the shell/spar nodes. This is particularly necessary in COBSTRAN as opposed to other programs, because of the special manner in which the program generates composite material properties at all grid points and then averages these properties among nodes defining an element in order to generate the material properties within each element. As such, the material properties of a grid point forming the boundary between the spar and the shell will contribute to the material properties of the elements on both sides of the boundary.

Modeling Strategy

The blade was designed as a fiber-glass/epoxy composite shell with an inner spar of solid aluminum. The area within the shell and outboard of the spar was filled with foam material. Spar and shell were bonded with a layer of adhesive and the leading edge was covered with a sheath of nickel. A typical cross section is shown in figure 6.

The material properties at each node were determined by evaluating each node as a series of layers of fiber-glass/epoxy, adhesive, and foam or aluminum with a symmetric stack-up through the thickness. The corresponding anisotropic stress-strain relations were calculated by laminate theory in which plane cross sections remain plane. Individual ply properties were calculated using micromechanics theory. Each node in the SR-7L model contained from 10 to 66 ply layers with a different ply stack-up order depending on the location of the node on the blade.

The COBSTRAN program is designed so that ply layers may be defined to exist over only specified areas of the blade expressed by a percent span and percent chord range (as shown in fig. 7). Making use of this feature, and repeated iterations through the COBSTRAN preprocessor, resulted in each of 326 nodes being defined by their correct thickness and ply order. Ply order is defined by sheath, shell, adhesive and foam or aluminum, as required, at each node location.

The shank of the blade was modeled using a bar element. The transition between the triangular plate bending elements of the blade and the bar element representing the shank was modeled by the use of multipoint constraints. The root of the shank was fixed in 4 degrees of freedom, the three translations and rotation about the spanwise axis. To represent the flexibility of the blade retention mechanism, rotation about both axes normal to span axis were represented by a rotational spring.

A normal modes analysis (MSC/NASTRAN solution sequence No. 3) was first performed to determine the first four natural frequencies and mode shapes at zero rotational speed.

Determination of steady state deflections, natural frequencies and mode shapes at selected rotational speeds was a more complex procedure. Because of the twist and sweep of the blade, steady state deflection calculations tend to be nonlinear. As such, the geometric nonlinear analysis capability available in MSC/NASTRAN was used (solution sequence No. 64). This procedure requires, as a minimum, two subcases to account for differential stiffness. Additional

subcases update the stiffness and mass matrices at each iteration. The number of additional subcases is problem dependent. For this analysis, eight additional subcases were determined to be sufficient to establish convergence.

A modification (DMAP alter) to the MSC/NASTRAN solution sequence No. 64 was made to prevent numerical instability. During the iteration the stiffness matrix tended to become singular due to very small values of rotational stiffness about the z-axis. To prevent this, for the first seven iterations the value of the stiffness matrix representing rotational stiffness about the z-axis was arbitrarily increased by a comparatively small value of 0.001. This additional stiffness was then excluded from the eighth and final iteration.

When calculating the stiffness matrix change in a centrifugal force field, MSC/NASTRAN does not account for the softening effects resulting from displacements in the plane of rotation. To obtain the correct frequencies and mode shapes, this softening effect must be included in the final stiffness matrix calculated in solution sequence No. 64. Therefore, a modification (DMAP alter) to the MSC/NASTRAN solution sequence was made to reduce the diagonal terms of the stiffness matrix associated with the translational degrees of freedom in the plane of rotation by a value of $(m \times \Omega^2)$. The final mass and stiffness matrices were stored by the MSC/NASTRAN database manager in temporary files for subsequent use by solution sequence No. 63, which is the normal modes analysis with database files.

The determination of ply stresses, strains and failure criteria is made possible by the use of the postprocessing feature of the COBSTRAN program. COBSTRAN accepts the element stress output from MSC/NASTRAN and calculates the stresses and corresponding membrane forces and bending moments at each node in the structural coordinate system. From these loads, using laminate theory, the resultant stresses, strains and failure criteria are calculated for each ply layer at each node in the ply coordinate system.

Steady State Deflections

The steady state deflections of SR-7L at cruise are shown in figure 8. The blade is loaded by centrifugal force and aerodynamic load, though the latter is small compared to the former. Since the blade is highly twisted, the contours are not shown in the global reference system. The contours represent deflections normal to a blade chord line at the three-fourths span position. As such, the deflections shown have very little edgewise component over the outer third of the blade where total deflections are the largest and are approximately normal to the blade in this region. The key feature of the deflection pattern is that while the peak deflections are small compared to the overall blade dimensions, the deflections and gradients tend toward "moderate" values relative to the outer part of the blade. This tendency is the result of the very thin blade construction, high centrifugal acceleration and built-in radial offset near the blade tip. Variations in any of these three factors can have a significant effect on the tip deflections. It is possible for tip deflections to vary significantly from blade to blade as a result of deviations from design in the fabrication of the blade tip. This is quite different from conventional straight propellers which are rugged along their entire length and essentially aligned with a radial vector so that centrifugal forces tend to restrict blade deflections, not induce them.

Natural Frequencies and Mode Shapes

The first four natural frequencies of SR-7L are shown on a Campbell diagram in figure 9. These span the frequencies of greatest concern with regard to flutter and forced response, although the first edgewise mode does not appear to contribute significantly to either. The Campbell diagram shows how the blade natural frequencies compare with engine order excitation frequencies as a function of the turboprop rotational speed. In order to avoid possibly severe dynamic response and subsequent fatigue damage, the critical blade natural frequencies should not be too close to an engine order excitation frequency (1-P, 2-P, etc.) near the turboprop operating speed. The "boxed-in" regions about each engine order are the exclusion zones near the operating speed. The lower engine order excitations, in general, tend to cause stronger blade forces and, as such, their respective exclusion zones are larger than for higher engine orders. As can be seen, the SR-7L, as designed, meets all frequency placement requirements with the possible exception of the fourth engine order interacting with the second bending mode. However, this interaction typically would not be anticipated to be strong and probably would not cause this particular blade design to be rejected.

Some special care must be taken in modeling blades like SR-7L for modal frequency analysis and in evaluating the results. Figure 10 shows the first four natural frequencies of SR-7L with and without a protective paint layer. This layer adds no stiffness to the blade but does add mass. Even though the layer is only 0.01 in thick, it increases the blade inertial properties by up to 10 percent near the tip. From this figure, the first three frequencies are effected only slightly by the paint layer. However, the fourth mode, first torsion, increased by about 3.5 percent when the paint layer was excluded from the model. Since modal frequency exclusion zones are typically about 5 percent of the natural frequency for high modes, variations of a few percent can be significant.

The mode shapes of the fully loaded SR-7L at the normal operating condition are shown in figure 11. The contour lines are, as with steady displacements, shown for deflections normal to the chordline at three-fourths span. The values of each contour line, subsequently, are properly scaled but represent arbitrary units for each mode.

The first mode appears as a "typical" blade first bending mode. The contour lines are essentially chordwise and are fairly evenly spaced along most of the blade span. The second mode is the first edgewise mode. Most of the motion in this mode is in the chordwise direction and, as such, is not shown by the contour lines in this figure. However, since this mode is not expected to contribute significantly to flutter or forced response, relative to the other modes shown, a detailed study of its motion is not needed for an analysis of SR-7L or similar blades.

The third mode is the second bending mode. The key feature of this mode is that most of the blade motion is in the outer third of the blade. Also, the contour lines tend to be in a chordwise direction. In some cases, swept blades of this type will have modal contour lines that slant downward from the leading edge of the blade to the trailing edge. Such blades will then have bending-torsion coupling which tends to be aeroelastically destabilizing and, thus, lowers the flutter speed. For the SR-7L analyzed here, the absence of any significant bending-torsion coupling should enhance the calculated stability boundary.

The fourth mode is a "typical" first torsion mode with a midchord mode line. The primary significance of this mode is that it couples with the bending mode aeroelastically to affect the stability of the blade. This form of coupling is not characteristic of unswept blades, in general.

Steady State Stresses

The steady-state stresses in SR-7L at the cruise condition are shown for the aluminum spar and fiberglass shell in figures 12 and 13, respectively. The regions with the highest stress are shown in both figures. In the spar, two regions exist with stresses over 10 000 psi. One region is on the pressure side of the blade near the bottom of the spar, and the other on the suction side of the blade toward the top of the spar. The lower region has a peak stress of 15 280 psi acting in a radial direction. The upper region has a peak stress of 15 050 psi, again in a radial direction. These stresses are dominantly bending, a result of the blade being offset from a radial line.

The shell also has two regions of high stress in approximately the same relative locations as for the spar. The shell is made from layers of cloth with a 0°, and -90° weave oriented in -30°, and +60° directions on the blade (as indicated in fig. 13). The cloth was subsequently modeled as two uniaxial layers, one in the -30° direction and the other in the 60° direction. Both regions encompass stresses over 3000 psi, and in both regions the highest stresses are in the -30° ply. The peak stress in the upper region is 6010 psi and the peak stress in the lower region is 6194 psi.

The peak stresses in both the spar and shell are relatively low and indicate that the cyclic stresses are below the allowable vibratory stresses.

CONCLUSIONS-STRUCTURAL ANALYSIS

Based on the structural analysis conducted during this study, several general conclusions can be drawn regarding the SR-7L advanced turboprop blade, in particular, and similar blades, in general:

(1) Blade deflections at cruise are structurally acceptable.

(2) Frequency margins relative to engine order excitations appear to be adequate (with the possible exception of the third mode, second bending, relative to the 4-P engine order).

(3) Steady-state stresses at cruise are acceptable.

(4) Blade deflections and critical vibration modes are dominated by motion of the comparatively thin outer portion of the blade (approximately the outer one-third). The results of the analysis and the actual behavior of the blade may be very sensitive to modeling and manufacturing detail in this portion of the blade.

AEROELASTIC ANALYSIS

Aeroelastic Methods

As previously mentioned, two computer codes were used to determine the aeroelastic characteristics of SR-7L. The major difference in these two codes is the type of structural model. These are a beam model and a finite element model for ASTROMIC and ACA/NASTRAN, respectively. ASTROMIC does have the advantage that it is easy and quick to use. ACA/NASTRAN is a modification of COSMIC NASTRAN generated by Bell Aerospace under a NASA contract. The extensive capabilities of this code allow it to be used as either a design/analysis or a research tool. Because ACA/NASTRAN is an extension of COSMIC NASTRAN, it can model complex structures. This capability makes the code well suited for modeling the structural configuration of a turboprop blade such as SR-7L. The disadvantage of using this code is that it requires a large amount of computer time and memory, resulting in lengthy computer runs. Also, the ACA/NASTRAN user must be fairly knowledgable in finite element techniques to prepare the extensive input data and to interpret the results.

The output from ACA/NASTRAN and ASTROMIC provide information about both the dynamic and aeroelastic characteristics of the turboprop blade. The dynamic characteristics supplied in the output are the natural frequencies and mode shapes. For the aeroelastic part of the analysis the programs output the aerodynamic damping for each mode of vibration. The flutter boundary is constructed by finding the locations of zero aerodynamic damping as a function of axial Mach number and rotational speed. The following sections give brief descriptions of the two methods.

Beam Method (ASTROMIC)

The details of the derivation of the beam method for unswept blades are given in reference 3. This method was developed for pretwisted, nonuniform blades by using Hamilton's principle. The derivation of the equations has its basis in the geometric nonlinear theory of elasticity in which elongations and shears are negligible compared to unity. A general expression for foreshortening (axial shortening of the tension axis due to bending, torsion, and noncoincidence of the elastic and tension axes) is explicitly used in the formulation. This method for unswept blades was modified in an approximate manner to account for blade sweep. For simplicity it was assumed that, although the blades are swept, the elastic axis is straight. Only the component of centrifugal load along the blade axis is considered. Also, for the flutter problem the blade is assumed to be vibrating about its undeformed position. The use of these assumptions can result in significant errors in the prediction of higher mode flutter characteristics. For example, it is known that proper consideration of the steady state displacements can cause the pure torsion mode (nonrotating) to change into a lower frequency, highly coupled bending-torsion mode. This modified version of the reference 3 method also has the capability to consider blade mistuning, but this is not considered herein.

Both subsonic (ref. 8) and supersonic (ref. 9) two-dimensional unsteady cascade aerodynamic theories are used. The assumed relative flow is the component normal to the elastic axes. The chord and stagger angle are also defined for sections normal to the elastic axis. The lift and moment are integrated in a stripwise manner to give a quasi-three-dimensional effect. These aerodynamic loads are corrected for sweep effects by using similarity

laws. This method, used in references 10 and 11 for an isolated, nonrotating, swept wing, involves modification of the two-dimensional lift and moment expressions for an unswept wing. The spanwise component of flow is neglected and similarities in the vertical velocity boundary conditions for swept and unswept wings are utilized.

The space variable in the resulting coupled integro-partial differential equations of motion is eliminated by using a modified Galerkin's method. The trial functions are the uniform beam mode shapes. For all results presented in this paper, two modes were used for each of three types of motion: bending in the plane of rotation, bending perpendicular to the plane of rotation, and torsion. The assumption of simple harmonic motion results in a generalized eigenvalue problem which is iteratively solved to determine the flutter boundary. Further descriptions of this analytical method can be found in references 3 and 12.

Finite Element Method (ACA/NASTRAN)

The detailed description of this method is given in references 4, 12 and 13. For the reader's convenience, a brief description follows. The method consists of three steps: (1) a "differential stiffness" matrix is determined from the steady state solution (by considering both centrifugal and steady aerodynamic loads and by using a Newton-Raphson iteration to determine the equilibrium position); (2) by using the additional stiffness from step 1, a free vibration analysis is performed to determine the modal characteristics; and (3) a modal flutter analysis is performed.

The two-dimensional, subsonic, cascade theory described in reference 14 is used to calculate the unsteady aerodynamic loads. The theories of references 8 and 14 are closely related and give similar results. A supersonic aerodynamic theory including sweep effects has yet to be incorporated into this method. The subsonic unsteady aerodynamic loads are modified to account for sweep effects by considering only the component of flow normal to the local leading edge. Although this method can include steady aerodynamic loads, they are not considered herein.

In general, a blade is a surface with multiple curvature. The method to form the aerodynamic forces for such a surface is as follows. For each station a "mean surface" is constructed between chord lines (which are normal to the leading edge and not parallel to each other) for this station and the adjacent spanwise locations (inboard and outboard). The modal translations normal to this surface are then used to construct the generalized aerodynamic force matrix.

As in the beam method, a complex generalized eigenvalue problem results. The flutter boundary is determined by repeated use of the "KE-Method" (ref. 15) for different axial Mach numbers and rotational speeds. Since this computer code presently lacks supersonic unsteady aerodynamics, the relative flow Mach number (perpendicular to the local leading edge) at all stations must be less than 1. This restricts the operating conditions at which this method can be used.

Previous Aeroelastic Analyses

Three other advanced turboprop designs (SR-5, SR-3 and SR-3C-X2) have been tested and analyzed for flutter. Since the conclusions and recommendations for SR-7L are related to the comparisons of these three experimental and analytical results, they will be briefly described.

SR-5 and SR-3 are solid metal (Ti) blades with different sweep distributions. The SR-3 blade has slightly more sweep than SR-7L while the SR-5 blade has about 15° more sweep. SR-3 and SR-3C-X2 have the same geometric shape but consist of different materials, solid metal (Ti) and graphite-epoxy, respectively. The ply orientations of SR-3C-X2 were specifically chosen to make the blade unstable within the capabilities of the experimental wind tunnel set up. The following sections will briefly describe the flutter analysis and experimental results for these three blades.

SR-5

A detailed description of the experimental results for SR-5 is given in reference 12. Also included in this reference are the results of a flutter analysis using the beam code which was described above. These results, assuming a constant sweep angle of 15°, are summarized in figure 14. As can be seen, there is only fair agreement between the experimental and analytical results. The overall experimental flutter boundary agrees well with the calculated boundary for a setting angle of 61°. A comparison of flutter boundaries for different setting angles shows the same trend. That is, increasing setting angle is a destabilizing effect. A comparison of flutter boundaries for similar setting angles shows only fair agreement between the experimental and calculated values. The calculated values always being somewhat conservative. It should be pointed out that the beam method is not expected to give precise values, since the structural model is not complete.

The SR-5 flutter analysis was repeated using the finite element method described previously. The finite element model for the blade is shown in figure 15. The rotating frequencies and mode shapes were first calculated by performing a geometrically nonlinear steady state analysis and then using the final stiffness matrix in a subsequent linear free vibration analysis. The centrifugal softening terms were included in both steps. The resulting Campbell diagram is shown in figure 16.

Also shown in the figure are experimentally determined natural frequencies (ref. 6). There is good agreement between the predicted and measured frequencies for the first two modes. These frequencies and mode shapes were used in the modal flutter analysis, ACA/NASTRAN. The resulting flutter boundary is shown in figure 17. As with the beam method, there is good agreement between the overall experimental flutter boundary and the calculated boundary. However, when similar setting angles are compared, the agreement is only fair. The beam and finite element method prediction are in good agreement and both are on the conservative side of the experimental boundary.

SR-3

The SR-3 model blades were examined for flutter susceptibility both experimentally and analytically. Within the capabilities of the wind tunnel, 11700 rpm and Mach 0.82, the blades were stable. The blade was analyzed using both the beam and finite element methods. The finite element model is shown in figure 18. The beam analysis was conducted assuming a constant sweep angle of 15°. In contrast to the experiment, both methods predicted flutter well within the test envelope. The predicted flutter boundaries are shown in figure 19. As can be seen, there is fair agreement between these methods for low rotational speed and poor agreement for high speed.

The beam method has the capability to consider both structural damping and mistuning (ref. 16). To determine the sensitivity of SR-3 to these two effects and possibly explain the discrepancy between analysis and experiment, additional flutter boundaries were calculated considering mistuning and damping separately. The results are shown in figure 19. The use of 0.5 percent structural damping resulted in a moderate effect on the flutter boundary, however, the blade was still predicted to flutter within the test envelope. The use of 10 percent alternate mistuning of the bending frequencies resulted in a stronger effect. The effect is strong enough to move the flutter boundary outside the test envelope. As a result of this study, it is concluded that neglecting mistuning and/or structural damping may cause the flutter predictions to be overly conservative.

SR-3C-X2

In addition to the solid metal SR-3, there is a family of blades with the same geometry but constructed of graphite/epoxy composite material. These blades are known as SR-3C. One set in this family, known as SR-3C-X2, was built-up with $\pm$22.5° ply orientations specifically designed to make the blade "flexible" and, hence, very susceptible to flutter. This set of blades was subjected to extensive wind tunnel testing and analysis. A subsequent publication will describe the experiments and analyses in detail, however, they will be summarized herein. The finite element model used was the same as in figure 18 for SR-3 but the material properties were obtained using COBSTRAN (ref. 2).

The experimental and analytical results are shown in figure 20. As can be seen, there is poor agreement. Once again, the analytical results are on the conservative side of the experimental flutter boundary. It should be mentioned that the analyses predicted the blade to be relatively insensitive to setting angle. The reasons for the very conservative nature of the analysis is an area of current study. Those areas being considered are mistuning, structural damping, three-dimensional aerodynamic effects (tip unloading and effective sweep), and transonic aerodynamic effects.

SR-7L FLUTTER ANALYSIS

ASTROMIC Analysis

Since the SR-7L blade has variable sweep and has spar/shell composite structure, equivalent beam properties must be estimated. Therefore, the COBSTRAN finite element model was used to calibrate the ASTROMIC SR-7L input

data. Adjustment was then made to ASTROMIC material properties in order to obtain good agreement in the first bending, second bending, and the first torsion modes (fig. 21). This approach was only good for these lower modes and starts to break down in the higher modes. ASTROMIC does a poor job of predicting the edgewise mode frequencies. This is seen in the large discrepancy between the codes for the first edgewise mode shown. The disagreement is attributed to the fact that ASTROMIC does not include shear deformation and rotary inertia.

Based on the geometric finite element model, the assumed straight elastic axis of SR-7L was swept 10°. This constant sweep angle resulted in the effective Mach number distribution shown in figure 22. Processing of the SR-7L input data results in the ASTROMIC modal damping predictions shown in figure 23. This figure displays the relationship between damping and flight Mach number at a specific operating condition (1700 rpm, sea level). The curve for this mode shows a sharp instability at 0.67 Mach number which would not be easily eliminated with increased damping. ASTROMIC predicted instability in the first mode only.

To assess the effect of altitude on the stability of SR-7L, the same ASTROMIC analysis was repeated at a constant rotational speed (1700 rpm) and various altitudes. This produced the ASTROMIC flutter boundary represented by the dashed line in figure 24. Increasing the altitude appears to have a stabilizing effect on SR-7L as can be seen by the movement of the flutter boundary to the right as altitude becomes higher. Ideally, no flutter prediction should occur to the left of the flight profile, but as can be seen in the figure, the flutter boundary crosses the flight envelope at 0.80 Mach number. This was not cause for concern in that ASTROMIC has been shown to underestimate the flutter speeds of SR-5. The reasons for this conservatism will be addressed later in this discussion.

ACA/NASTRAN Analysis

The effective Mach number used by ACA/NASTRAN differs considerably from that used in ASTROMIC. The difference comes from the way that the aerodynamic loads are corrected for the blade sweep. While ASTROMIC is limited to a constant sweep angle (straight elastic axis), ACA/NASTRAN can account for the actual variation in the blade sweep. The effective Mach number in ACA/NASTRAN is taken as perpendicular to the leading edge and will thus change not only with the rotational velocity component but also with the sweep angle. The effective Mach number distribution for SR-7L for ACA/NASTRAN, along with that of ASTROMIC is shown in figure 22.

ACA/NASTRAN is restricted in that it does not have transonic or supersonic capability and, therefore, cannot handle relative Mach numbers of 0.95 or greater. With this limitation and the specified rotational speed of 1700 rpm, the maximum flight Mach number is fixed at 0.88. Figure 25 presents damping as a function of flight Mach number for three modes at four flight speeds (0.40, 0.60, 0.80 and 0.88 Mach numbers) and at a constant rotational speed of 1700 rpm (sea level). Neither mode one or three approaches instability at 0.88 Mach number. Mode two is a predominantly edgewise bending mode for which the aerodynamic loads are always small.

Referring once again to the flight envelope depicted in figure 24, the ACA/NASTRAN aeroelastic analysis of SR-7L was performed at 1700 rpm with various altitude conditions. No instability could be found up through the maximum Mach number (M = 0.88) capability of the code.

The results generated by both ASTROMIC and ACA/NASTRAN for SR-7L are believed to be conservative. First, damping was not included in the analysis. Disregarding damping is conservative since both material and mechanical (such as root friction) damping are known to have a stabilizing effect on flutter. Second, blade mistuning was neglected. Results from previous studies on the effect of mistuning (ref. 17) indicate that a moderate amount of mistuning can alleviate flutter problems. Third, both ASTROMIC and ACA/NASTRAN use two-dimensional aerodynamic theories which assume that there are an infinite number of blade cross sections out the span. This assumption does not allow for the inclusion of tip unloading effects which would be included were a full three-dimensional aerodynamic theory used. These three dimensional effects have been shown to move the flutter boundary to a higher operating condition. Neglecting the three-dimensional effects results in lower operating speed flutter predictions. The final reason for conservatism is the limitations of the computer codes in their abilities to realistically simulate the transonic effects. Both codes use a less than adequate estimation of the transonic effects which appears to result in conservative flutter predictions.

CONCLUSION-AEROELASTIC ANALYSIS

1. As previously described, the agreement between analytical and experimental flutter boundaries has ranged from fair to poor. However, the analytical predictions have always been on the conservative side; that is, the predicted flutter Mach number has always been less than that measured in the wind tunnel. The suspected reasons for this conservatism have been discussed.

2. SR-7L is predicted to be stable over the entire flight envelope by the finite element method. The more approximate beam method predicts this blade to be stable over most of the flight envelope. A small region in the upper right hand corner is unstable. In light of these predictions and the knowledge of the conservative nature of the analytical predictions, the SR-7L is judged to be a low risk aeroelastically.

SUMMARY OF RESULTS

Four separate analyses were performed on the SR-7L advanced turboprop blade: (1) a steady state deflection analysis; (2) a modal analysis; (3) a steady state stress analysis; and (4) an aeroelastic stability analysis. The first three analyses, forming a complete structural analysis, were based on a large deflection finite element analysis. The aeroelastic analysis used two independent approaches: (1) an approximate beam analysis, and (2) a refined finite element analysis. This study found the SR-7L blade to be structurally sound and aeroelastically stable. However, there are generic characteristics of blades of this type which can cause less carefully designed blades to be structurally and aeroelastically unacceptable.

First, most of steady state deflections and vibratory motion occur in the outer third of the blade which is very thin. This part of the blade is also heavily loaded and, as such, the blade tip undergoes geometrically moderate

deflections. Also, due to sweep the blade can have a degree of vibratory pitch-flap coupling which is detrimental to stability.

Because the blade is so thin, small deviations from design specifications during fabrication can have a significant effect on the overall blade characteristics. This was demonstrated by comparing the blade natural frequencies with and without a thin protective paint layer. This layer caused one of the critical natural frequencies to change by 3.6 percent. Considering that resonance margins are only about 5 percent, a variation of this size can be significant. As a result, special attention must be given to designing, analyzing and fabricating the outer portion of blades like SR-7L.

It was also found during this study that the flutter boundaries predicted by the approximate and refined analyses differed significantly, though the overall analysis indicated that the blade would be stable over its entire proposed flight envelope. While the approximate beam analysis predicted some flutter at high Mach numbers and altitudes, the more refined analysis, with a better structural and aerodynamic model, predicted no flutter. Subsequently, the approximate analysis proved to be a good tool for qualitatively examining the aeroelastic stability of SR-7L but is not adequate for a detailed study of such a complex blade. For that matter, even the refined analysis has deficiencies in that three-dimensional aerodynamic tip effects, transonic effects and structural damping are not included. However, these effects tend to improve stability, and as such, the aeroelastic analysis conducted can be considered conservative.

In conclusion, while this study found the SR-7L advanced turboprop blade to be structurally sound and aeroelastically stable, special care must be taken when designing, analyzing and fabricating blades of this type. Also, though the analysis methods used in this study proved to be adequate for SR-7L, there is room for considerable improvement in methodology for structurally and aeroelastically analyzing advanced turboprop blades, as well as in construction and fabrication concepts.

REFERENCES

1. Dugan, James F., et al: The NASA High-Speed Turboprop Program. NASA TM-81561, 1980.

2. Chamis, Christos C.: Integrated Analysis of Engine Structures. NASA TM-82713, 1981.

3. Kaza, K.R.V.; and Kielb, R.E.: Flutter of Turbofan Rotors with Mistuned Blades. AIAA J., vol. 22, no. 11, Nov. 1984, pp. 148-1625.

4. Elchuri, V; and Smith, G.C.C.: Flutter Analysis of Advanced Turbopropellers. AIAA 83-0846, 1983.

5. Hirschbein, M.S.; and Brown, K.W.: STAEBL - Structural Tailoring of Engine Blades (Phase II). Presented at the Symposium on Recent Experiences in Multidisciplinary Analysis and Optimization, (NASA Langley Research Center, Langley, VA), Apr. 24-26, 1984.

6. Srinivasan, A.V; and Fulton, G.B.: Advanced Turboprop Vibratory Characteristics. (United Technologies Research Center; NASA Contract NAS3-23533.) NASA CR-174708, 1984.

7. Aiello, Robert A.; and Chamis, Christos C.: Large Displacement and Stability Analysis of Nonlinear Propeller Structures. NASA TM-82850, 1982.

8. Smith, S.N.: Discrete Frequency Sound Generation in Axial Flow Turbomachines. R&M no. 3709, British A.R.C., 1973.

9. Adamcyzk, J.J.; and Goldstein, M.E.: Unsteady Flow in a Supersonic Cascade with Subsonic Leading-Edge Locus. AIAA J., vol. 16, no. 12, Dec. 1978, pp. 1248-1254.

10. Barmby, J.G.; Cunningham, H.J.; and Garrick, I. E.: Study of Effects of Sweep on the Flutter of Cantilever Wings. NACA TN-2121, 1950.

11. Bisplinghoff, Raymond L.; Ashley, Holt, and Halfman, Robert L.: Aeroelasticity. Addison-Wesley Publishing Co., 1955.

12. Mehmed, O., et al.: Bending-Torsion Flutter of a Highly Swept Advanced Turboprop. NASA TM-82975, 1982.

13. Smith, G.C.C.; and Elchuri, V.: Aeroelastic and Dynamic Finite Element Analysis of a Bladed Shrouded Disc. (Textron Bell Aerospace Co.; NASA Contract NAS3-20382.) NASA CR-159728, 1980.

14. Rao, B.M.; and Jones, W.F.: Unsteady Airloads on a Cascade of Staggered Blades in Subsonic Flow. Unsteady Phenomena in Turbomachinery, AGARD CP-117.

15. The NASTRAN Theoretical Manual. NASA SP-221 (06), Jan. 1981.

16. Kielb, R.E.; and Kaza, K. R.V.: Aeroelastic Characteristics of a Cascade of Mistuned Blades in Subsonic and Supersonic Flows. Journal of Vibration, Acoustics, Stress and Reliability in Design, vol. 105, no. 4, Oct. 1983, pp. 425-433.

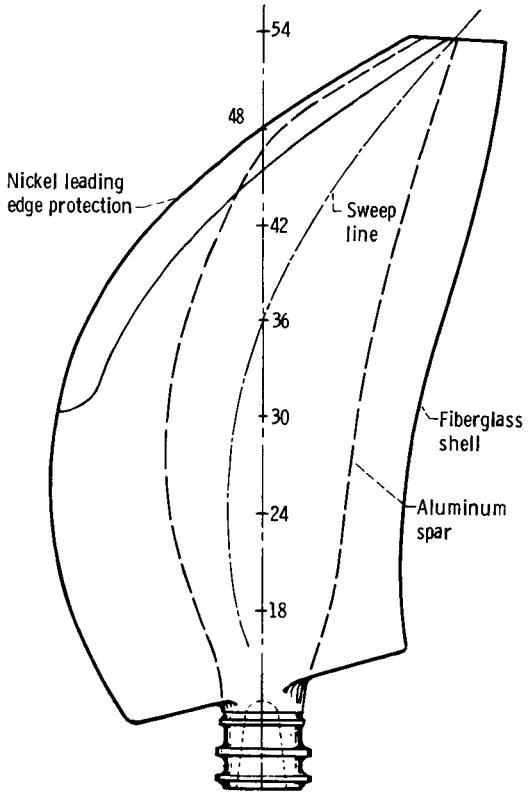

Figure 1. - SR-7L turboprop blade.

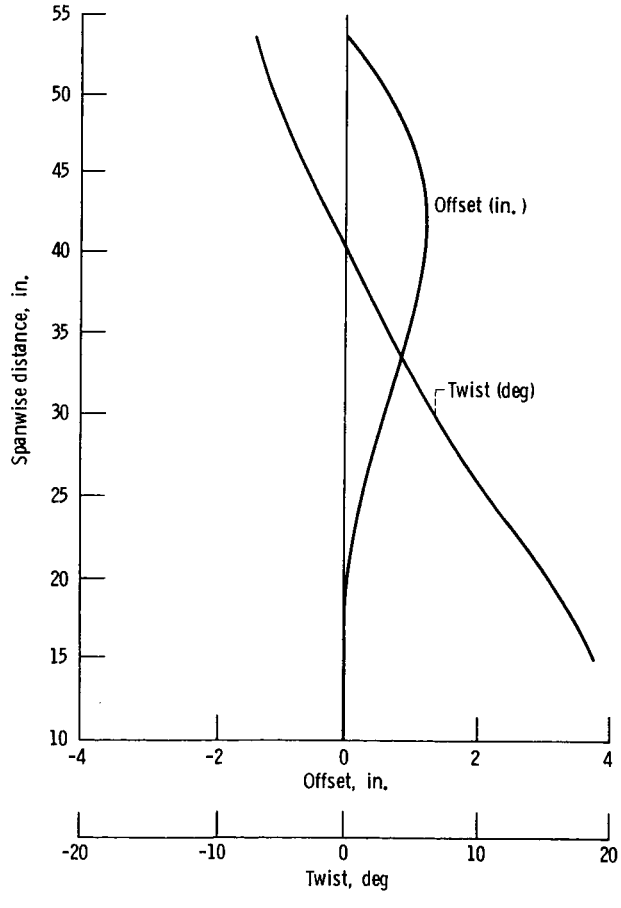

Figure 2. - SR-7L twist and offset.

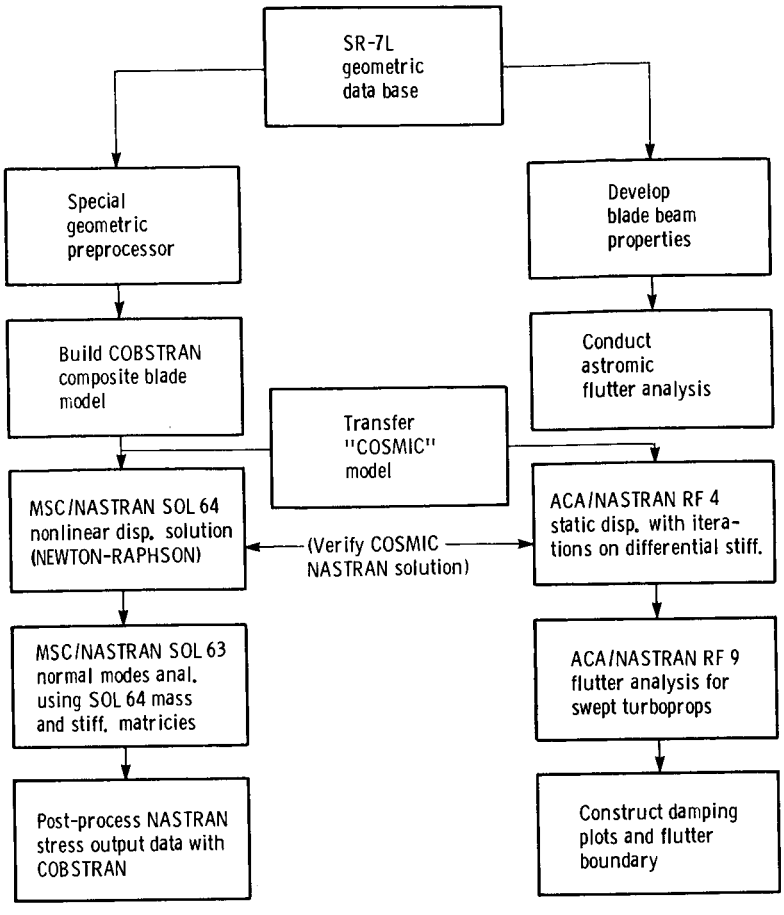

Figure 3. - Analytical procedure.

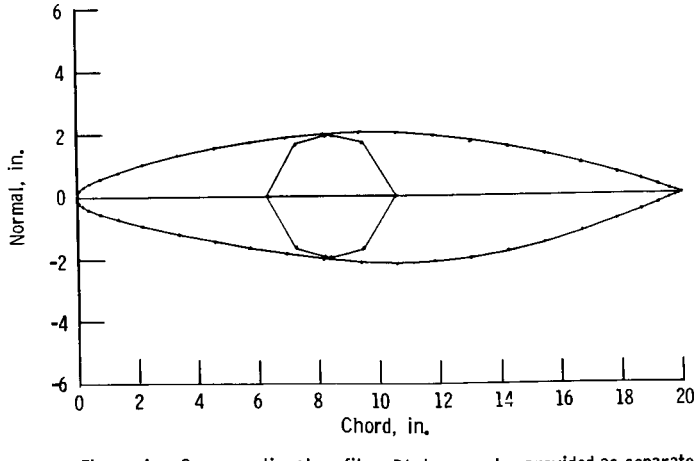

Figure 4. - Cross-sectional profile. Blade geometry provided as separate profiles for spar outline and shell mid-thickness.

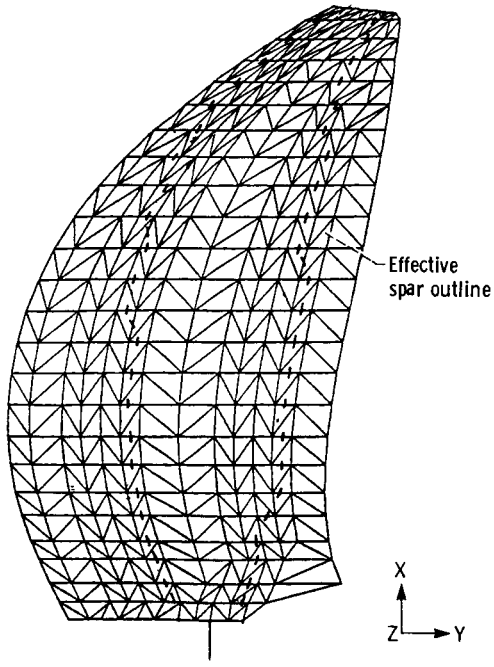

Figure 5. - COBSTRAN finite element model. Nodes, 328; elements, 584.

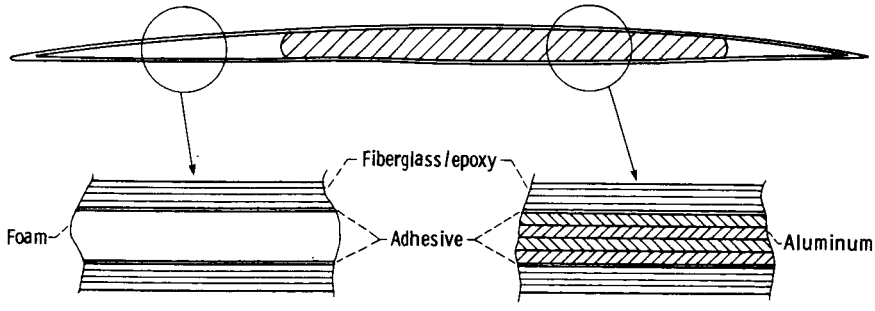

Figure 6. - Typical blade cross-section.

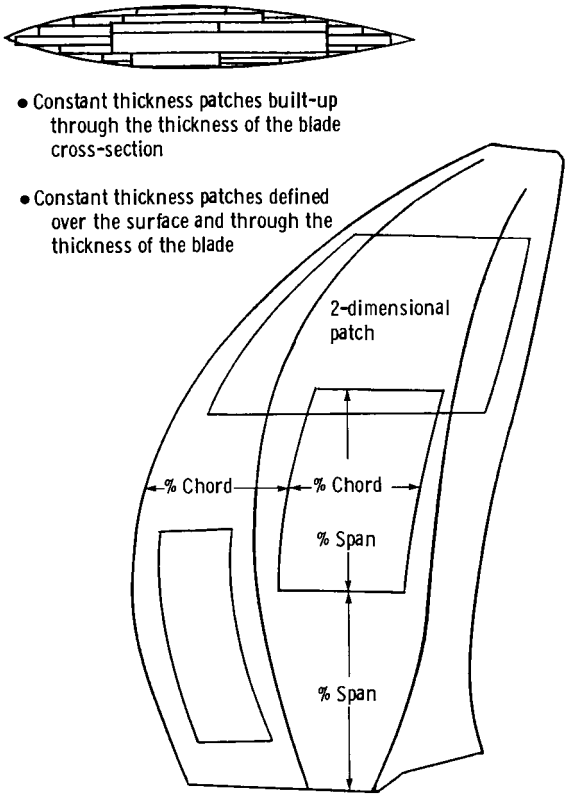

Figure 7. - COBSTRAN laminated plate model.

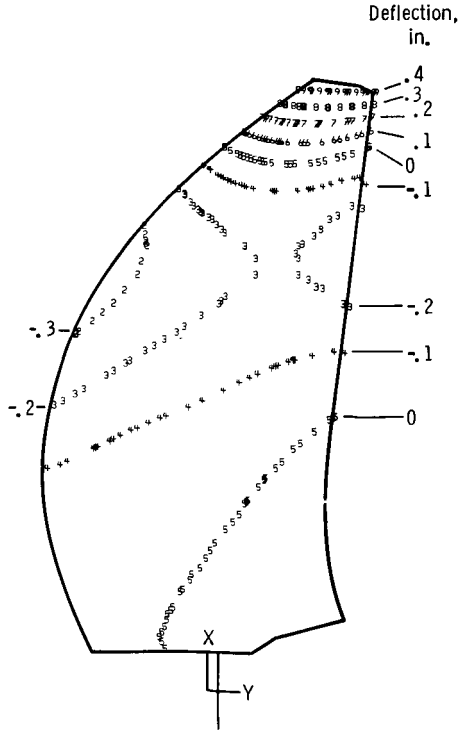

Figure 8. - Steady deflections at cruise conditions (1700 rpm with air loads).

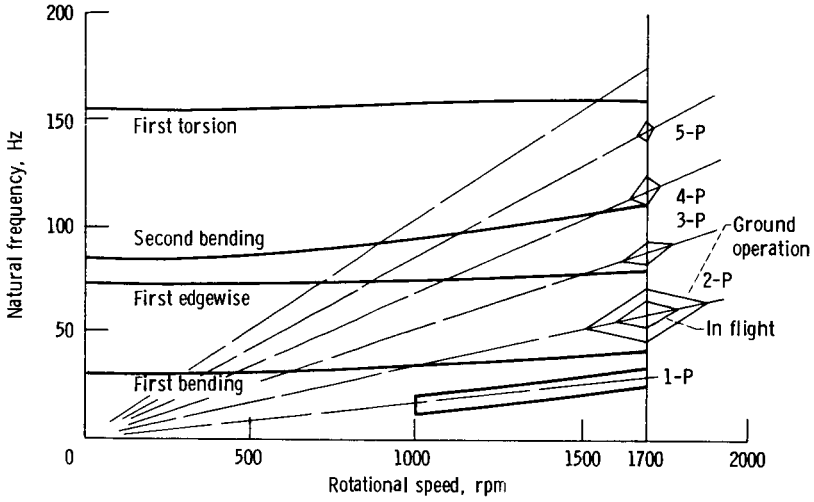

Figure 9. - Campbell diagram.

NATURAL FREQUENCIES AT 1700 rpm

MODE	MSC NASTRAN (WITH PAINT), Hz	MSC NASTRAN (WITHOUT PAINT), Hz
FIRST BENDING	41.8	42.3
FIRST EDGEWISE	72.9	73.9
SECOND BENDING	111.6	113.2
FIRST TORSION	160.9	164.3

Figure 10. - Effect of protective paint layer on natural frequencies.

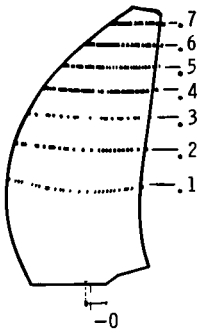

(a) First mode, 41.8 Hz, first bending.

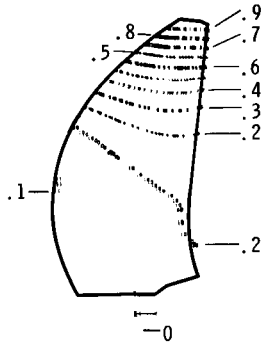

(b) Second mode, 72.9 Hz, first edgewise.

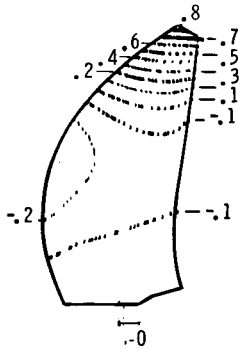

(c) Third mode, 111.6 Hz, second bending.

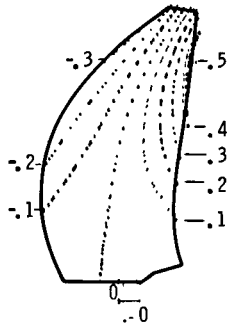

(d) Fourth mode, 160.9 Hz, first torsion.

Figure 11. - Natural mode shapes. (Contour lines are arbitrary units normal to the blade chord at the 3/4 span position.)

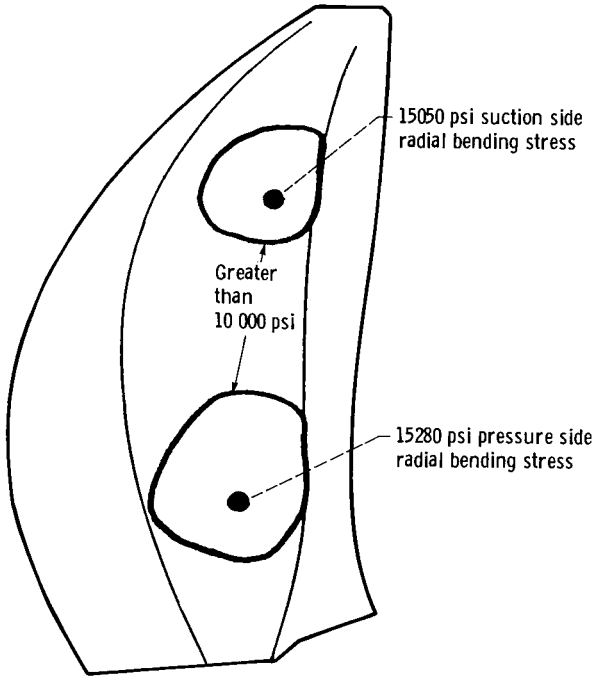

Figure 12. - Regions of highest spar stress.

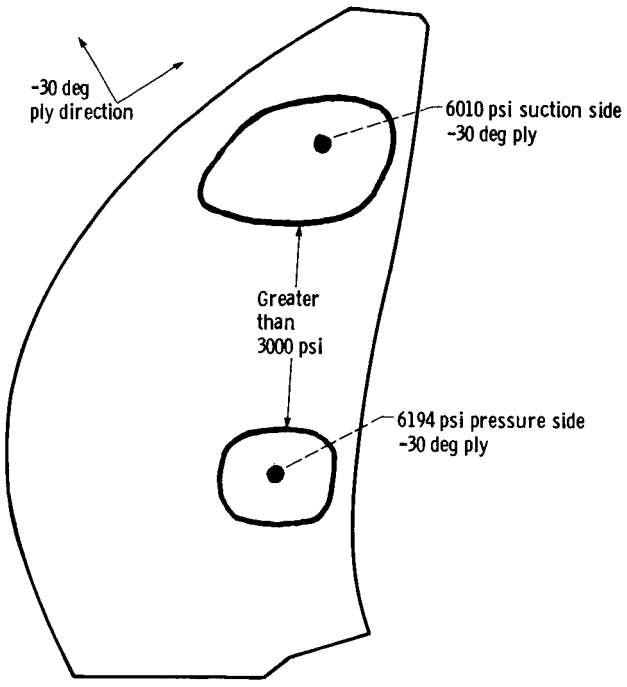

Figure 13. - Regions of highest shell stress.

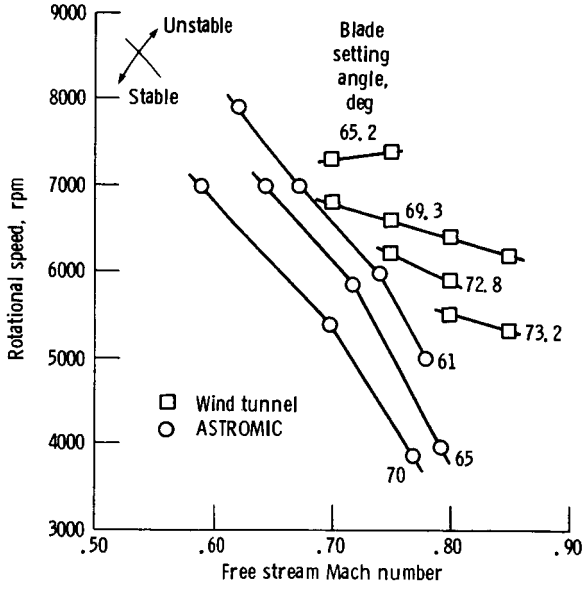

Figure 14. - SR-5 flutter data.

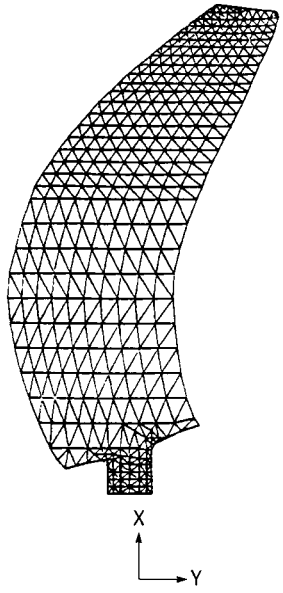

Figure 15. - SR-5 finite element model.

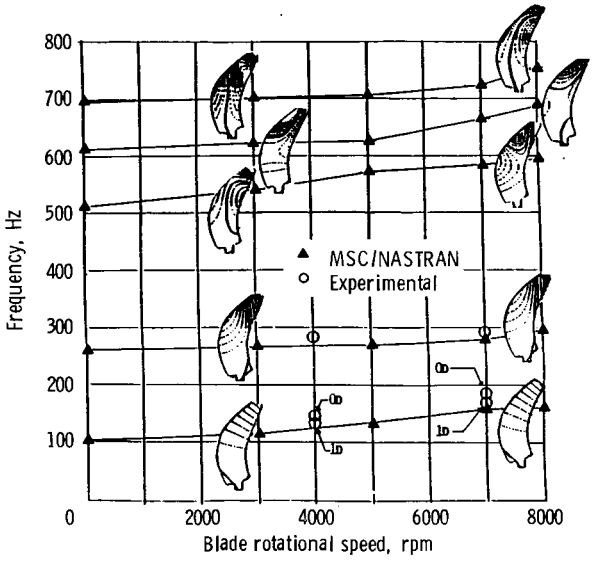

Figure 16. - SR-5 Campbell diagram.

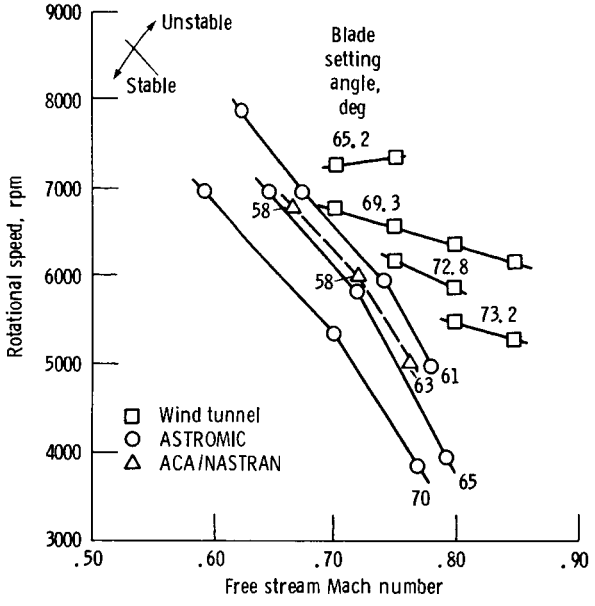

Figure 17. - SR-5 flutter boundary.

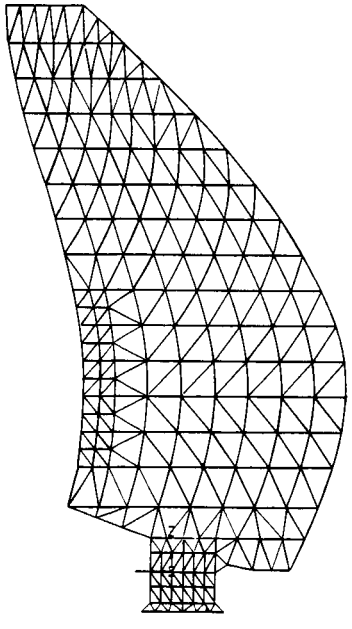

Figure 18. - SR-3 finite element model.

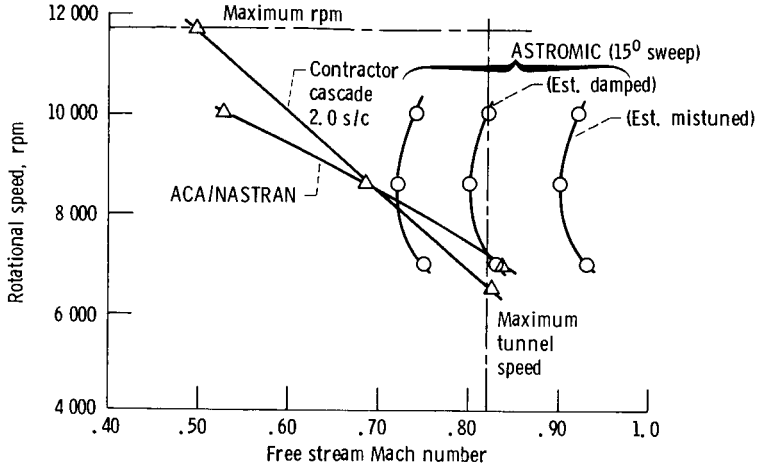

Figure 19. - SR-3 flutter data.

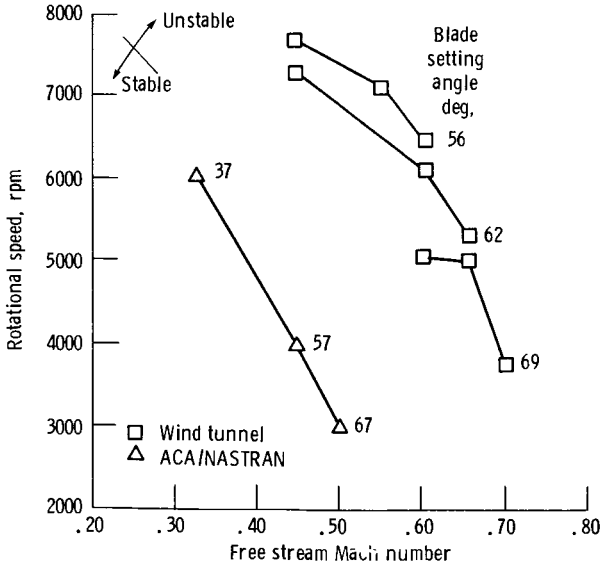

Figure 20. - SR-3C-X2 flutter boundary.

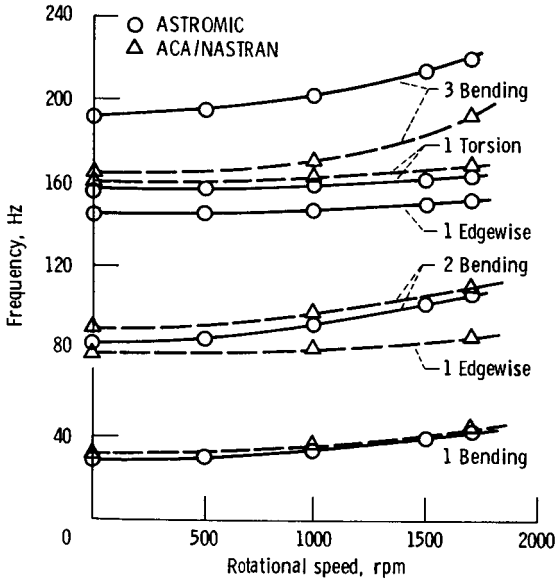

Figure 21. - Comparison of ASTROMIC and ACA/NASTRAN natural frequencies.

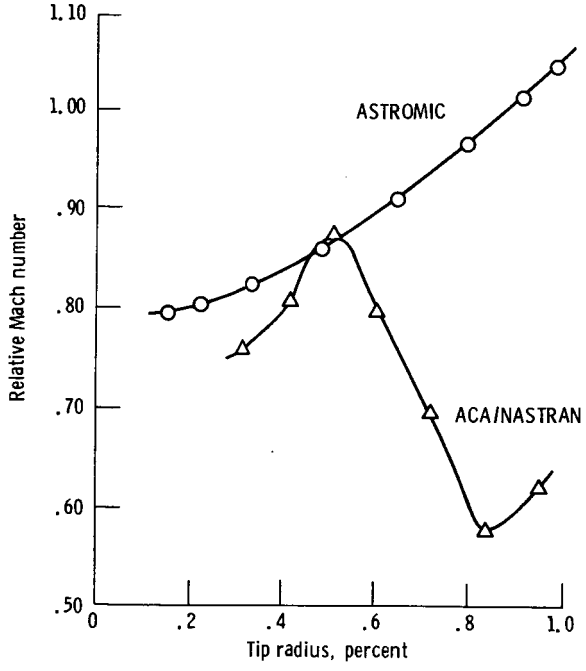

Figure 22. - Effective Mach number distortion.

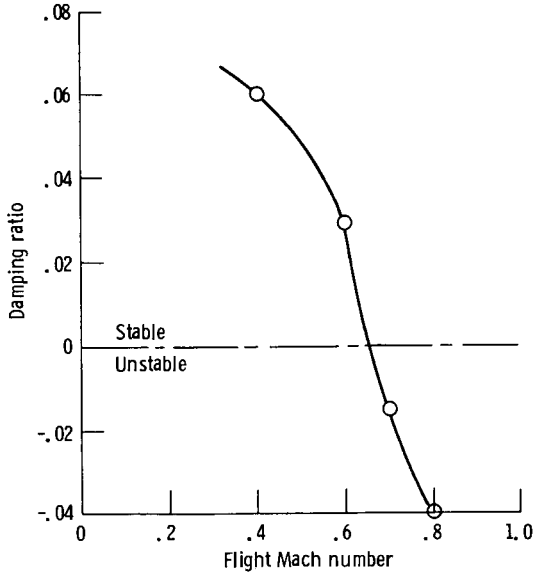

Figure 23. - ASTROMIC modal damping. First bending; rotational speed, 1700 rpm.

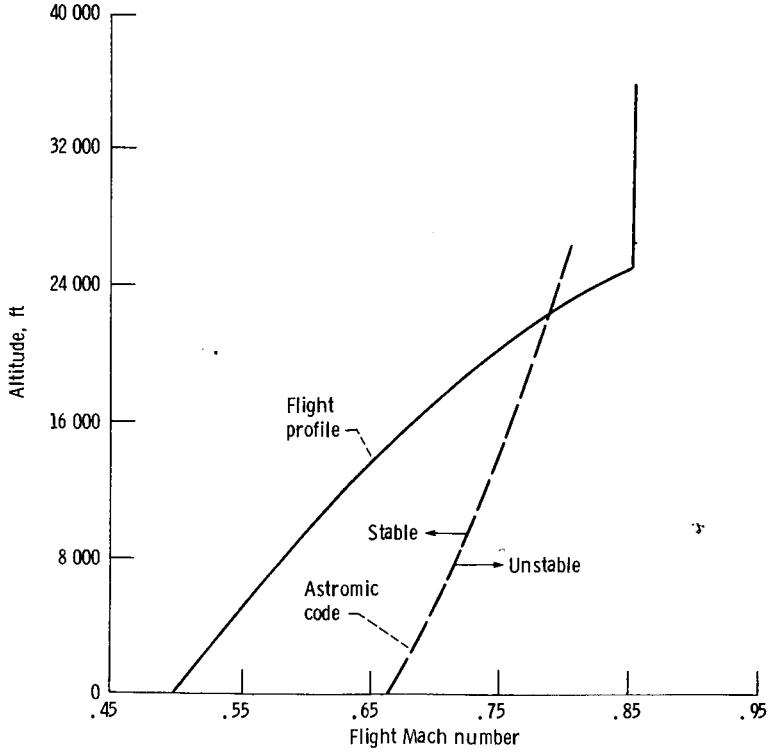

Figure 24. - SR-7L flight profile and ASTROMIC stability boundary. Rotational speed, 1700 rpm.

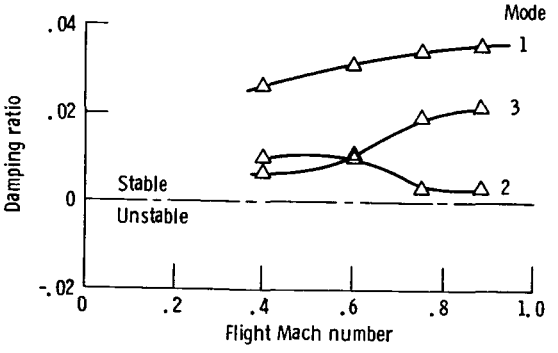

Figure 25. - ACA/NATRAN modal damping. Rotational speed, 1700 rpm.

1. Report No.	2. Government Accession No.	3. Recipient's Catalog No.
NASA TM-86877		

4. Title and Subtitle	5. Report Date
Structural and Aeroelastic Analysis of the SR-7L Propfan	March 1985
	6. Performing Organization Code: 535-03-12

7. Author(s)	8. Performing Organization Report No.
Murray Hirschbein, Robert Kielb, Robert Aiello, Marsha Nall, and Charles Lawrence	E-2338
	10. Work Unit No.

9. Performing Organization Name and Address	11. Contract or Grant No.
National Aeronautics and Space Adminstration Lewis Research Center Cleveland, Ohio 44135	
	13. Type of Report and Period Covered: Technical Memorandum

12. Sponsoring Agency Name and Address	14. Sponsoring Agency Code
National Aeronautics and Space Administration Washington, D.C. 20546	

15. Supplementary Notes

16. Abstract

This paper presents a structural and aeroelastic analysis of a large scale advanced turboprop rotor blade. This 8-blade rotor is designed to operate at Mach 0.8 at an altitude of 35 000 ft. The blades are highly swept and twisted and of spar/shell construction. Due to the complexity of the blade geometry and its high performance, it is subjected to much higher loads and tends to be much less stable than conventional blades. Four specific analyses were conducted: (1) steady deflection; (2) natural frequencies and mode shapes; (3) steady stresses; and (4) aeroelastic stability. State-of-the-art methods were used to analyze the blades including a large deflection, finite element structural analysis and an aeroelastic analysis including interblade aerodynamic coupling (cascade effects). The study found the blade to be structurally sound and aeroelastically stable. However, it clearly indicated that advanced turboprop blades are much less robust than conventional blades and must be analyzed and fabricated much more carefully in order to assure that they are structurally sound and aeroelastically stable.

17. Key Words (Suggested by Author(s))	18. Distribution Statement
Structures Flutter Propellers	Unclassified - [redacted] STAR Category 39

19. Security Classif. (of this report)	20. Security Classif. (of this page)	21. No. of pages	22. Price*
Unclassified	Unclassified		

*For sale by the National Technical Information Service, Springfield, Virginia 22161